INTERFACE

rsif.royalsocietypublishing.org

Research

Cite this article: Sareh S, Althoefer K, Li M, Noh Y, Tramacere F, Sareh P, Mazzolai B, Kovac M. 2017 Anchoring like octopus: biologically inspired soft artificial sucker. *J. R. Soc. Interface* **14**: 20170395.
http://dx.doi.org/10.1098/rsif.2017.0395

Received: 30 May 2017
Accepted: 27 September 2017

Subject Category:
Life Sciences–Engineering interface

Subject Areas:
biomimetics

Keywords:
soft robotics, robotic anchoring module, stiffness-gradient design, single sensory unit, seamless measurement, tactile sensing

Author for correspondence:
Sina Sareh
e-mail: sina.sareh@rca.ac.uk

THE ROYAL SOCIETY
PUBLISHING

Anchoring like octopus: biologically inspired soft artificial sucker

Sina Sareh[1], Kaspar Althoefer[2], Min Li[3], Yohan Noh[4], Francesca Tramacere[5], Pooya Sareh[6], Barbara Mazzolai[5] and Mirko Kovac[6]

[1]Design Robotics, School of Design, Royal College of Art, London, UK
[2]Advanced Robotics @ Queen Mary (ARQ), Faculty of Science & Engineering, Queen Mary University of London, London, UK
[3]Institute of Intelligent Measurement & Instrument, School of Mechanical Engineering, Xi'an Jiaotong University, Xi'an People's Republic of China
[4]Centre for Robotics Research, Department of Informatics, King's College London, London, UK
[5]Center for Micro-BioRobotics, Istituto Italiano di Tecnologia, Pontedera, Italy
[6]Aerial Robotics Laboratory, Department of Aeronautics, Imperial College London, London, UK

SS, 0000-0002-9787-1798; PS, 0000-0003-1836-2598

This paper presents a robotic anchoring module, a sensorized mechanism for attachment to the environment that can be integrated into robots to enable or enhance various functions such as robot mobility, remaining on location or its ability to manipulate objects. The body of the anchoring module consists of two portions with a mechanical stiffness transition from hard to soft. The hard portion is capable of containing vacuum pressure used for actuation while the soft portion is highly conformable to create a seal to contact surfaces. The module is integrated with a single sensory unit which exploits a fibre-optic sensing principle to seamlessly measure proximity and tactile information for use in robot motion planning as well as measuring the state of firmness of its anchor. In an experiment, a variable set of physical loads representing the weights of potential robot bodies were attached to the module and its ability to maintain the anchor was quantified under constant and variable vacuum pressure signals. The experiment shows the effectiveness of the module in quantifying the state of firmness of the anchor and discriminating between different amounts of physical loads attached to it. The proposed anchoring module can enable many industrial and medical applications where attachment to environment is of crucial importance for robot control.

1. Introduction

A sensory–physical system is the integration of a physical process with sensors and computation enabling monitoring or the control of the process. A robotic anchoring module is a sensory–physical mechanism for attachment to the environment. Robotic anchoring modules with the ability of maintaining their attachment for an extended time duration would be invaluable for a wide range of industrial and medical applications: attachment in climbing robots for inspection and cleaning of huge glass walls, nuclear plants and steel bridges, perching in flying robots that can provide a bird-eye view of an area of interest or object manipulation and attachment into delicate substrates, e.g. human body. However, often degradation and failure of attachment mechanisms cause unwanted detachment from the contact surface indicating the need for continuous monitoring of the firmness of the anchor during the robot mission. Moreover, precise control of the robot requires information about the contact surfaces located within the proximity of the robot anchoring module(s).

Anchoring into well-grounded structures is a biologically inspired approach for locomotion, stiffness control, object manipulation, standing against fluid flows and energy management in animals. One of the most common strategies in nature to obtain reversible attachment is using a specialized organ known as a sucker. Such an organ allows fish, annelids, helminths and cephalod molluscs to anchor onto a variety of substrates including rough, flexible and dirty surfaces.

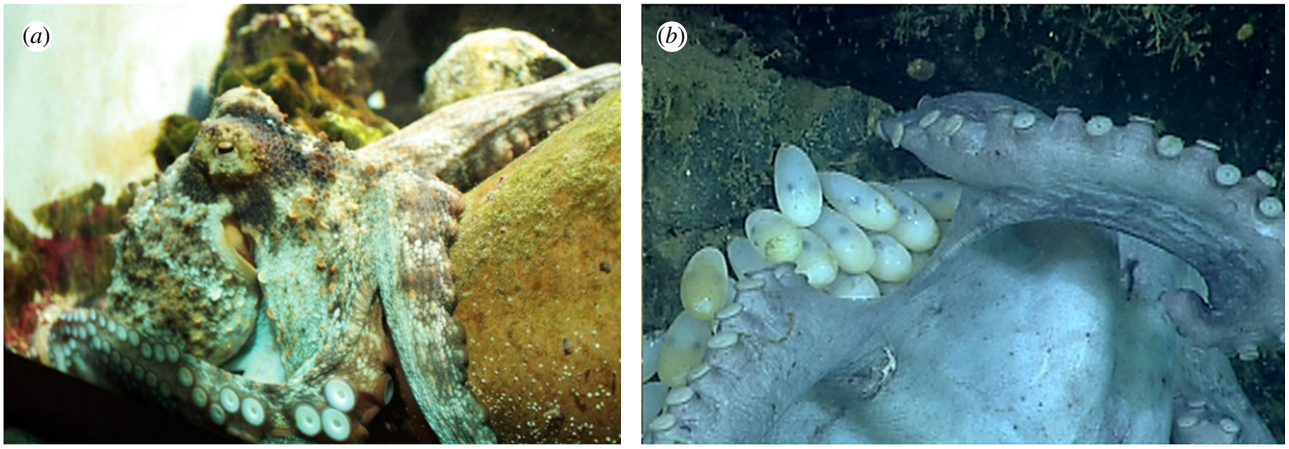

Figure 1. Octopuses use rows of sensory suckers to attach to objects with varying degrees of force. This includes the use of suckers for (*a*) anchoring to hard objects, such as rocks, to stand against storm surge and waves [15], as well as (*b*) manipulating delicate or soft objects, such as octopus egg capsules [15]. (Reproduced under a Creative Commons Attribution License from [16].) (Online version in colour.)

This attachment organ demonstrates effectiveness both in terrestrial and aquatic environments. In gobies, e.g. blackeye goby *Rhinogobiops nicholsii*, the fused pelvic fins form a disc-shaped sucker used to anchor to substrata or bigger fish [1]. The northern clingfish, *Gobiesox maeandricus*, has an adhesive disc on its ventral side that allows the animal to attach on smooth surfaces as well as very rough surfaces to resist against strong water currents [2]. The leeches, which can be found both in terrestrial and aquatic environments, are characterized by the same attachment organs, one anterior and one posterior sucker [3–7]. A coordinated activation and deactivation of suckers enables directional movement in leech. The tapeworm *Taenia solium* (parasite of human gut) uses four suckers around the head to approach the gut wall and a set of hooks to fix onto it [8,9]. Most prominently, octopus arms are equipped with one or two rows of suckers [10] that are controlled independently [11]. These sophisticated organs can attach to objects with varying degrees of force. This includes anchoring to perfectly smooth surfaces as well as to surfaces with a certain roughness [12], where technical suction cups usually fail [2]. The suckers of benthic octopuses can enable multiple functionalities [12] including locomotion [13], chemotactile recognition [14], anchoring the body to hard substrates (figure 1*a*) by which standing against storm surge and waves [12,15,17], as well as grasping and manipulation of small objects (even soft and delicate objects such as their egg capsules) [12,16], as can be perceived from figure 1*b*.

In living organisms, nature has evolved combined abilities of perceiving the location of approaching objects and applied forces after interacting with them. For example, in big brown bat *Eptesicus fuscus* sound waves and echos are used to estimate their distance from approaching objects, a technique known as echolocation. Once touching the object, the animal relies on the tactile information provided by merkel cells[1] within its wings [18,19]. The two modes of perception are analogous to proximity and tactile sensing in robotic systems. Since any touch occurs after an approaching event, the tactile and proximity sensing are regarded as complementary [20], where a combination of both sensing modalities enables continuous perception from an approaching event to a following touching event. In robotic anchoring systems, tactile information can enable ranking the firmness of the anchor(s) to the objects, while proximity information can assist in robot motion planning prior to the touching event.

Biomimetic aspects of octopus suckers have been long studied; the morphology and physiology of octopus suckers and possibilities for biomimetic replication of suckers have been investigated [12,16,21–25], with particular emphasis on the transition from hard to soft in the mechanical stiffness of sucker [21–25], also referred as stiffness-gradient[2] design in some relevant literature [26,27].

A number of researchers have proposed passive artificial suckers [25], and actuated suckers using shape memory alloy [28] and dielectric elastomer actuators [29]. The existing literature on sensorization of artificial suckers is predominantly relevant to the development of smart skins for robotic arms to inform the robot about its interaction with the environment. In this context, tactile sensing elements based on quantum tunneling composite (QTC) materials and conductive textiles were proposed in [30,31]. However, the sensitivity of the prototype drops by increasing the area of the QTC pill[3] [30]. In another effort a thin layer of silicone with a hole at the centre was sandwiched between two sheets of Electrolycra and integrated underneath an artificial sucker to measure compressive tactile forces [31]. In this paper, we leverage the previous work on stiffness gradient [26,27] design of octopus suckers [25] and integrate it with a single sensory unit which can seamlessly measure both tactile and proximity information.

2. Material and methods

2.1. Bioinspired stiffness-gradient design of the anchoring module

The mechanical design of the anchoring module is taking inspiration from the biology of octopus sucker described in figure 2*a*,*b*. The octopus sucker consists of two functional parts linked through a constricting orifice (figure 2*b*): the infundibulum, the outer funnel-like portion of the sucker, and the acetabulum, the inner hollow portion. When a sucker attaches itself to an arbitrary surface, e.g. a rock, the infundibulum adapts its shape to that surface creating a seal and reduces its thickness by contracting the radial muscles, thereby increasing the attachment to the surface. Consequently, the contraction of the acetabular radial muscles [12] reduces the pressure inside the sucker and generates attachment [16,21–25]. In fact, with water being an incompressible medium, the contraction of the acetabular muscles put the water inside the sucker in tension, resulting in a reduction of internal pressure. The higher the levels of muscle contraction in

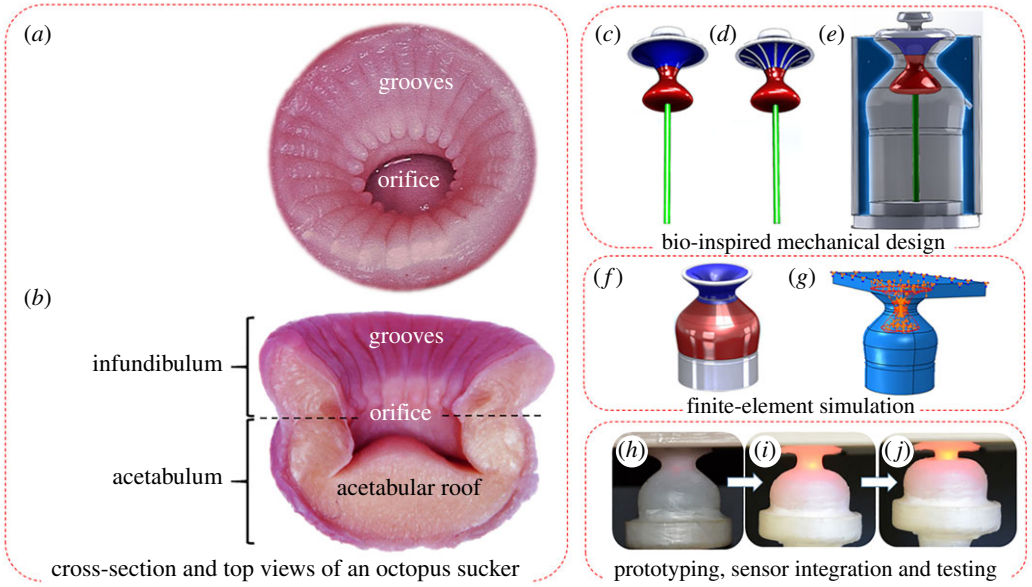

Figure 2. An overview of the methodology for bioinspired design and implementation of the anchoring module. (*a*) The top view of an octopus sucker with grooves on the surface of the infundibular portion. These radial grooves not only allow the pressure generated in the acetabular chamber to be transmitted to nearly the whole sucker–substrate interface thereby increasing the firmness of the anchor, but also facilitate the detachment process. (*b*) The cross section of the sucker showing its biological structure. (*c*) CAD design of the internal part of moulds without groove structures. Note that the straight rod in the mould's CAD model creates a channel for an optical fibre to be passed through at a later stage. (*d*) CAD design of the internal part taking into account the radial grooves in the natural suckers (number of grooves = 12, depth and width of grooves = 500 µm). (*e*) The external part of the mould. (*f*) The CAD design of the anchoring module with an infundibular part (blue), an acetabular part (red), and a rigid base creating a stable platform for testing (silver). (*g*) The FEA Abaqus simulation models the vacuum pressure inside the anchoring module as a uniformly distributed pressure load. (*h*) The fabricated anchoring module featuring a stiffness gradient in its mechanical structure is held tangent to the contact surface (vacuum input and sensor: off). (*i*, *j*) The gradual attachment to the contact surface (vacuum input and sensor: on). (Online version in colour.)

the acetabulum, the higher are the values of difference of pressure, resulting in a firmer attachment.

In [21–25] the structure and mechanical properties of the natural sucker were extensively investigated and a set of principles for the bioinspired design of an artificial sucker was concluded. In order to mimic the conformability of the infundibulum, this portion must be fabricated from a soft and sticky material. Similarly, the artificial acetabulum must be made from an elastic and stiffer material in comparison with infundibulum. To enhance the efficiency of the artificial sucker in attachment and detachment processes, the bioinspired design of the artificial infundibulum should also take into account the grooves of the natural infundibulum surface (figure 2*a*). The radial grooves create channels for guiding the pressure generated in the acetabulum to nearly the whole interface between the sucker and the contact surface to obtain a stronger attachment and faster detachment. Therefore, a mechanical stiffness gradient and appropriate channels for transmission of the acetabular pressure to the sucker–substrate interface are central to the mechanical design of the anchoring module, as an artificial sucker, and were considered for bioinspired replication as a part of this study.

In line with these design objectives, we developed a set of 3D CAD models of moulds required for material casting and fabrication of the anchoring module, presented in figure 2*c–e*; the moulds consists of an internal core which shapes the internal cavities and radial grooves, and an external housing. In this study, the radial grooves are 500 µm wide and 500 µm deep, and are equally distributed (every 30°). Each groove has a triangular shape radially diverging from the aperture of the orifice to the edge of the infundibulum. The moulds were 3D printed using a rapid prototyping machine.[4]

In this study, two types of silicone materials, Ecoflex® 00–30 and Dragon Skin® 00–10,[5] were considered for stiffness-gradient fabrication of acetabular and infundibular parts of the anchoring module (Ecoflex® 00–30 is softer than Dragon Skin® 0010). Yeoh model [32] was used to simulate the hyperelastic behaviour [33] of the two materials from uniaxial extension test data [34], expressed as

$$U = \sum_{i=1}^{3} C_{i0}(\bar{I}_1 - 3)^i + \sum_{i=1}^{3} \frac{1}{D_i}(J^{el} - 1)^{2i}, \qquad (2.1)$$

where U is the strain energy per unit of reference volume, C_{i0} and D_i are the material parameters [32], $\bar{I}_1$ is the first deviatoric strain invariant[6] and J^{el} is the elastic volume ratio. In order to further simplify the model, we assume incompressibility of the two materials, and hence the second term of the Yeoh model (equation (2.1)) can be neglected. Therefore,

$$U = C_{10}(\bar{I}_1 - 3) + C_{20}(\bar{I}_1 - 3)^2 + C_{30}(\bar{I}_1 - 3)^3 \qquad (2.2)$$

is used for simulation. The respective material parameters are listed in table 1 [34].

The CAD parts of the anchoring module were imported into Abaqus FEA[7] as homogenous solid elements. Then, a set of finite-element simulations, as reported in §3, were run to evaluate the attachment and detachment performance of anchoring module when a soft–hard gradient architecture in the material stiffness is used. The imported CAD model (figure 2*f*) was discretized into solid hexahedral linear reduced integration elements (Abaqus mesh type C3D8R) with a mesh size of 2.5 mm. The anchoring module was modelled as an assembly of the infundibulum and acetabulum parts, and a 'tie' type constraint (the constraint prevents any relative motions between two parts of the assembly) was used to bond these two parts. Note that as a part of the model, a flat plate (figure 2*g*) representing the surface onto which the anchoring system should attach is created

Table 1. The material parameters of Ecoflex® 00–30 and Dragon Skin® 00–10 [24,34].

elastic parameters	mass density (tonne/mm^3)	elastic modulus (MPa)	hyperelasticity	Poisson's ratio	C_{10} (MPa)	C_{20} (MPa)	C_{30} (MPa)
Ecoflex® 00–30	1.07×10^{-9}	34.8 ± 2.7	uniaxial test data	0.4	7.61×10^{-3}	2.42×10^{-4}	-6.2×10^{-7}
Dragon skin® 00–10	1.07×10^{-9}	129.0 ± 9.7	uniaxial test data	0.4	36×10^{-3}	2.58×10^{-5}	-5.6×10^{-7}

and placed above the anchoring module (the Young's modulus of the plate is 1100 MPa). The top surface of the plate was set to be fixed during the simulation. The vacuum pressure inside the anchoring module was modelled using a uniformly distributed pressure load. The FEA model was used to simulate the loading capabilities and deformation of the anchoring module under variable amounts of vacuum pressure. Figure 2*h–j* shows the prototype of the anchoring module with integrated sensing system, explained in the next section, undergoing the attachment process.

2.2. Sensory–physical design of the module: seamless measurement of tactile and proximity information

The complementary roles of proximity and tactile sensors in robotic sensing has led to a number of efforts to integrate both capabilities into a single sensory unit to minimize the overall hardware and satisfy the requirements (e.g. weight and size) for integration into a wider range of robotic systems including light-weight flying robots and compact manipulators for operation in confined spaces. To date, prominent examples of such sensing systems include capacitive tactile proximity sensors based on silver nanowires and polymer film [35] and carbon microcoils [36]. Since the former uses the same capacitive range for both proximity and tactile sensing, the sensor is not able to distinguish between static proximity and tactile inputs. The later requires a control circuit for switching between two modes of operation.

The diffuse-reflective fibre optic systems [37–40], which exploit the light intensity modulation sensing principle [37–43], can potentially provide better opportunities for seamless measurement of tactile and proximity information in practical applications. The non-contact nature of the sensing principle enables performing the measurements independent of the geometry of the embodying structure and the actuation system and, hence, no action is required for transition between the two modes of sensing. Also, the simple and independent structure of these sensors makes them more durable and robust for operation over an extended time period. The fibre optic sensors are free of electrical current in the sensing site making them inherently safe for integration into anchoring modules that can potentially be attached to vulnerable substrates or human body. Moreover, they are suitable for integration into soft robotic systems, because the flexibility of optical fibre can preserve the inherent softness of this class of robots [39–41].

The sensory system of our anchoring module exploits light intensity modulation, as described in figure 3*a*, occurring between a reflective fibre unit FU-69U[9], which is embedded inside the artificial acetabulum (figure 3*b*), and the contact surface. In this paper, the distance a between the optical fibre tip and the contact surface, specified in figure 3*b*, is referred as 'anchor length'. During the attachment, as the anchor length is reduced, the intensity of the reflected light is increased (figure 3*c*) indicating a firmer attachment. A FS-N11MN fibre-optic sensor from the same optical manufacturer was used to convert the light intensity into voltage information, subsequently acquired by a NI USB 6211[10] data acquisition card. Although the sensor system is not immune to the external light, it is highly resistant to the ambient light (unaffected for up to 30 000 lux) [44]. The sensor arrangement is able to measure an anchor length within 40 mm of the optical fibre tip [44]. Note that our work on the sensing system aimed at replicating two biological functions (proximity and tactile sensing) using a single sensory unit, as opposed to replicating biological sensing principles.

In order to calibrate the single sensory unit of the anchoring module, the module was integrated into a custom calibration device using a mounting shaft (figure 3*d*). The calibration device consists of a motorized linear guide and a motion controller which allows modulating the anchor length in an automated and repeatable manner between 2 and 40 mm, while the voltage output from FS-N11MN fibre optic sensor is recorded, as can be perceived from figure 3*c*,*d*. The sensor is calibrated for two different contact surfaces made from aluminium (mill finish) and wood (oak finish) materials, and the calibration curves are presented in figure 3*e*.

The anchor length can be calculated through

$$a(\text{mm}) = \frac{p_1}{v^3 + q_1 v^2 + q_2 v + q_3}, \tag{2.3}$$

where v is the analogue output voltage acquired from the FS-N11MN and p_1, q_1, q_2 and q_3 are calibration coefficients that are described in table 2. It should be mentioned that equation (2.3) presents a rational fit to the voltage-anchor length data worked out in Matlab.[11]

2.3. Fabrication, mechatronics integration and testing of the anchoring module

In order to fabricate the anchoring module, the mould shown in figure 2*e* was placed upside down and the Ecoflex® 00–30 material was poured into it until reaching a full coverage of the infundibulum area, and then heated at 55°C for 20 min inside an oven. Subsequently, the Dragon Skin® 00–10 material was added into the mould until reaching a three millimetre thick acetabular roof (it should be mentioned that both silicone materials were degassed inside a vacuum chamber prior to the casting process). At this stage, the FU-69U four-core optical fibre and a 2 mm (outer diameter) vacuum pipe were embedded inside the acetabulum as shown in figure 4, and the workpiece was left at room temperature (approx. 25°C), to be cured overnight. A 3D printed plastic base was then glued to the bottom of the anchoring module to ensure that the position of the optical

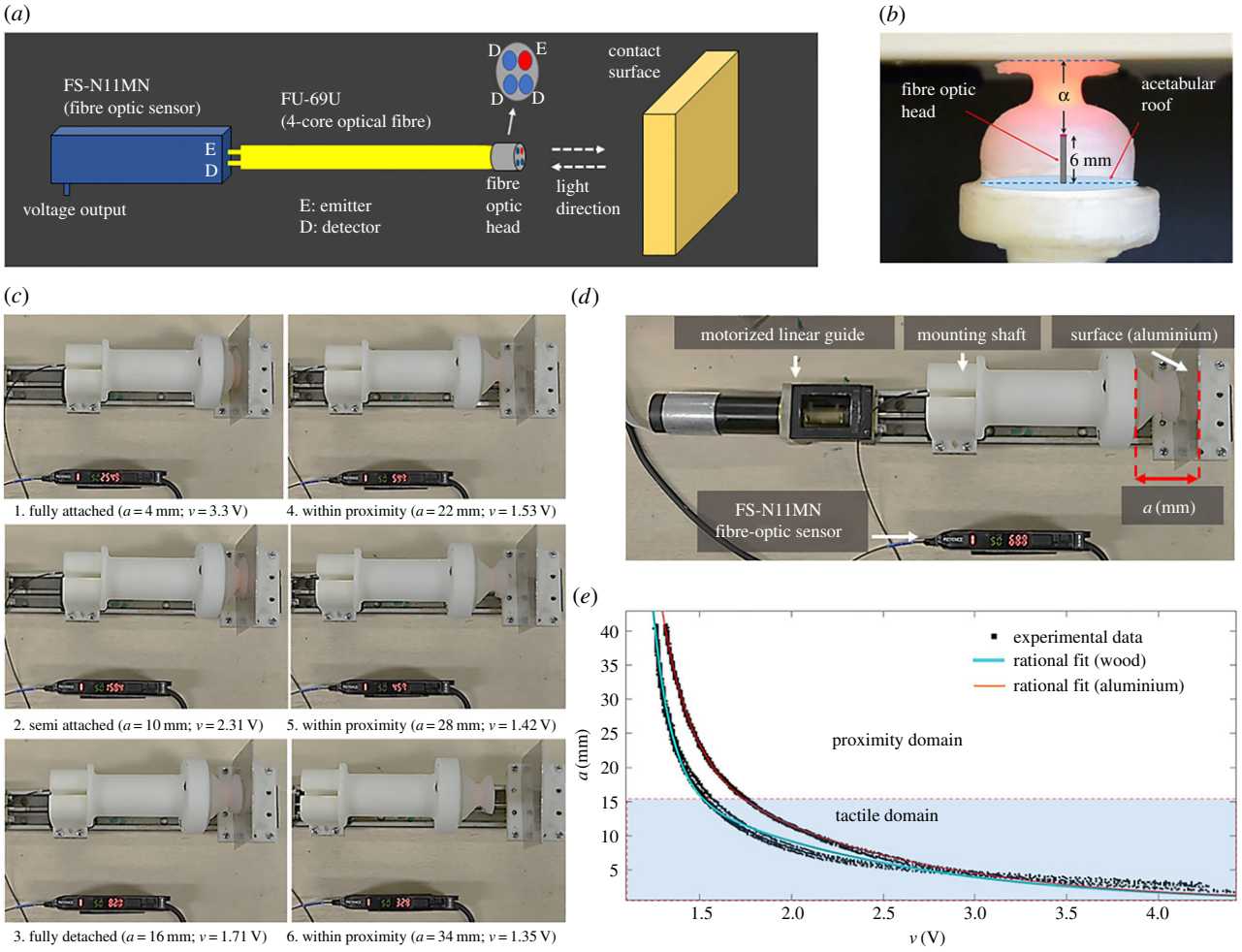

Figure 3. (*a*) The configuration of the diffusive–reflective fibre optic system consisting of a light source and detector module (FS-N11MN fibre optic sensor) and a four-core optical fibre unit. (*b*) The definition of the anchor length α. (*c*) Seamless calibration of the anchoring module's sensing system; the module is integrated with a motorized linear guide and a custom[8] motor control software which enables running repeated experiments automatically; note the change in sensor reading while the anchoring module is moving away from the contact surface. (*d*) Description of the experimental setup and parameters. (*e*) The proximity and tactile domains of the calibration curve for wood and aluminium materials as described by equation (2.3). (Online version in colour.)

Table 2. The curve fitting coefficients for aluminium and wood materials.

coefficients	p_1	q_1	q_2	q_3
aluminium	52.94	−5.179	13.72	−10.05
wood	49.99	−7.313	22.11	−16.99

fibre is kept fixed during successive experiments, providing a stable platform for experimentation.

The overall configuration of the anchoring module consisted of soft artificial infundibulum and acetabulum parts integrated with the four-core optical fibre and the vacuum supply pipe, as shown in figure 4. The vacuum pressure was supplied by a Mastercool 90066 vacuum pump via an ITV0090-2BN-Q vacuum regulator with an onboard pressure sensor. Analogue voltage values corresponding to the vacuum pressure and the light intensity were transferred to a computer via the data acquisition system.

As a comparison with the natural counterpart, it is worth noting that at sea level an octopus can create a pressure differential ranging from 100 to 200 kPa using its sucker mechanism. However, the animal is able to generate higher pressure differentials at greater depths, where the water pressure is higher [12]. When the anchoring module is operating in air, the pressure differential cannot exceed the limit of 1 bar (100 kPa), because the absolute negative pressure is not possible except for solids and liquids [45]. Note that in this study all experiments were performed in air.

3. Results and discussion

3.1. Characterization of maximum loading capacity

In order to evaluate the actuation capabilities of the anchoring module, its maximum loading capacity under different values of vacuum pressure inputs ranging from −0.1 bar to −0.5 bar was quantified. The results of the respective finite-element simulations and experimental results imply that the anchor can be maintained for physical loads up to around 2 N (figure 5*a*). In another experiment, the actuation of the anchoring module with a fixed total weight of 1.09 N was captured using a high-resolution video camera. The anchor length for different values of vacuum pressure inputs was calculated from video images and compared with the respective simulation results. The experiment was repeated five times and the results are plotted in figure 5*b* indicating a maximum error of 27% between simulated and experimental values of anchor length. The error can be mainly due to possible inaccuracies in the uniaxial test data; the specimens used for the uniaxial test in [34] and our experimental prototype were all fabricated through similar manual casting processes.

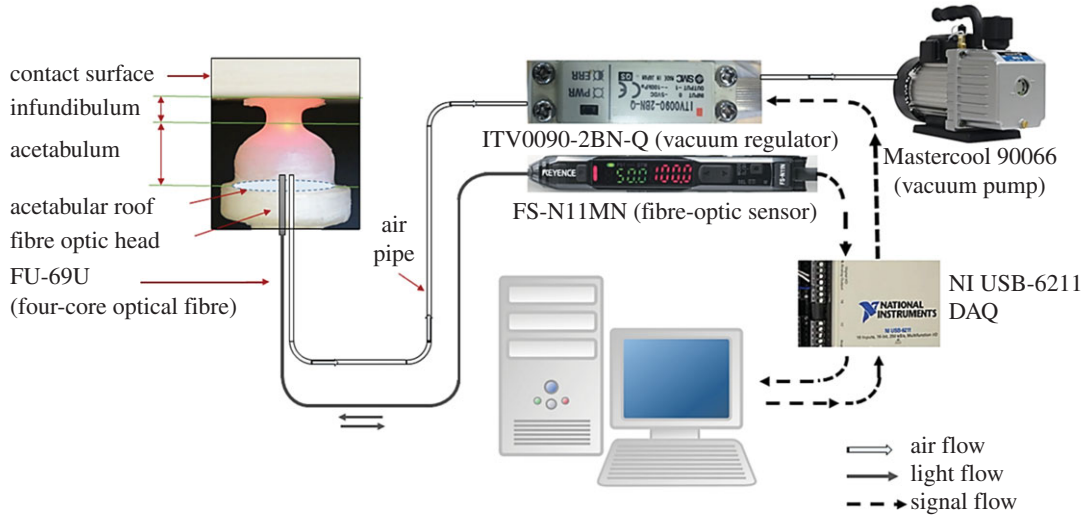

Figure 4. The mechatronic configuration of the sensory–physical anchoring module. The module features a stiffness-gradient design in its mechanical structure and was actuated using a Mastercool 90066 vacuum pump via an ITV0090-2BN-Q vacuum regulator. The system was able to seamlessly measure tactile and proximity information using a single sensory unit consisting of an FU-69U four-core fibre optic unit and an FS-N11MN fibre optic sensor. (Online version in colour.)

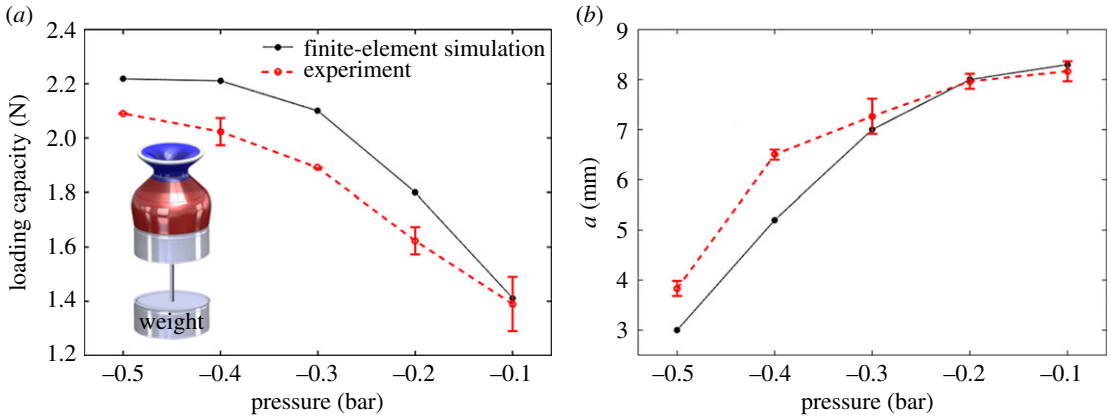

Figure 5. The finite-element simulation and respective experimental results for attachment to a wooden surface. (*a*) Loading capacity versus pressure; the maximum amount of physical load that can keep the anchoring module connected to the surface at different pressures was simulated in Abaqus FEA and physically experimented. Note that the inset shows the setup for adding physical load to the module while it was vertically attached to a surface. (*b*) Anchor length versus pressure; the results of the finite-element simulations were compared with the respective data extracted from camera images. (Online version in colour.)

Hence, there can be some differences in material properties due to the quality of manual fabrication. Other sources for the error can be related to the hyperelastic model used for simulation as well as experimental measurements.

3.2. Dynamics of the reversible anchoring system and firmness of the anchor

The ability of the sensing system in quantifying the firmness of the anchor under different physical loading conditions was evaluated. In order to be able to perform multiple cycles of experiments consistently, we defined a minimum value for the input pressure signal which guarantees for the anchoring system to be attached to the wooden surface during the whole course of experiment, where additional weights were stacked up on top of existing loads (see the inset in figure 5*a*) and the sensor output was recorded. This minimum value was −0.1 bar which was determined by the experiment in §3.1 and figure 5*a*. Hence, a reverse sawtooth vacuum input with respective maximum and minimum values of −1 and −0.1 bar was applied to the anchoring module (figure 6*a*). The weight of the anchoring module was gradually increased by adding additional standard calibration slotted weights to the bottom of the module to reach an overall weight of $W = \{0.69, 0.89, 1.09\}$N (in successive experiments) and the sensor signals (figure 6*b*) were analysed in accordance with visual information from camera images. In figure 6*c* the respective anchor lengths were calculated from equation (2.3) and the correspondence to the key sequences of detachment (1–4, figure 6*d*) was indicated, under a physical load of 1.09 N. Note that figure 6*e* shows the complete detachment if we reduce the vacuum signal to 0. It can be perceived from figure 6*b* that the sensor's reading starts decreasing from the higher value of 4.67 V (representing a firm anchor), until reaching a minimum value of 1.77 V (representing a vulnerable anchor) during the detachment process. The camera images show a slight swing of the anchoring module around the anchor point during the detachment process that is due to the torque generated by the added weights to the bottom of the module; this can explain the temporary drop of the sensing voltage, in figure 6*b*, to the curve's minimum value of 1.77 V before settling at a higher value of 2.08 V, e.g. for a physical load of 1.09 N (note that the swing of the anchoring module

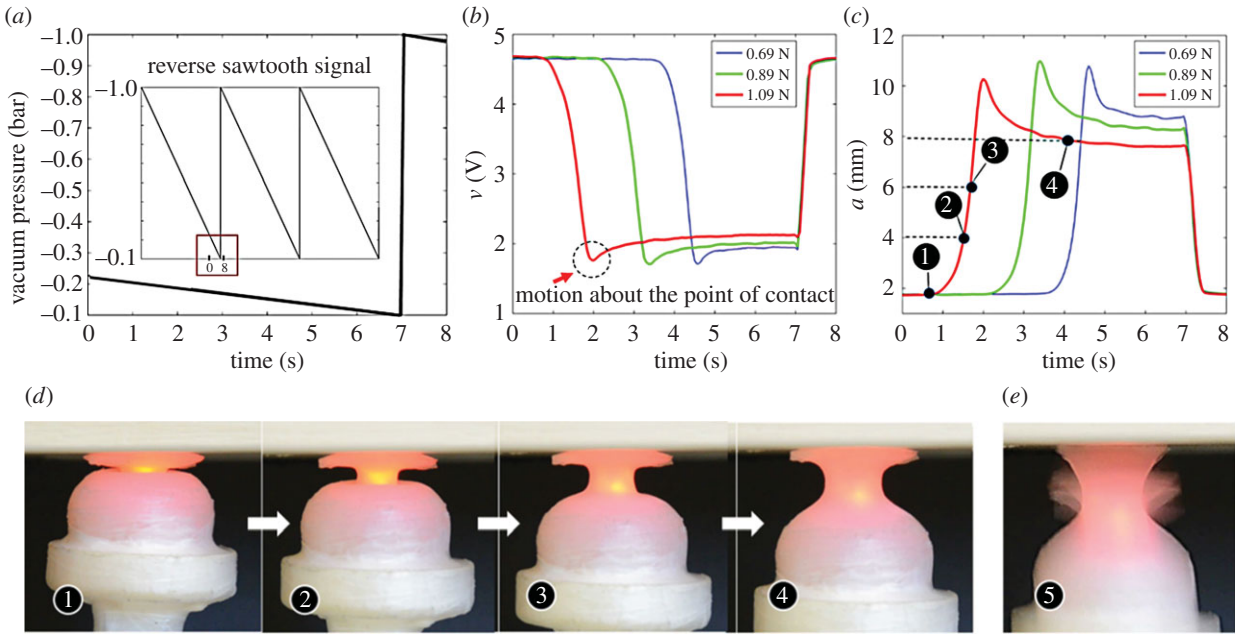

Figure 6. (*a*) The reverse sawtooth input signal with maximum and minimum values −1 and −0.1 bar (this signal is a part of the full reverse sawtooth signal shown in the inset with a period of 50 s). It should be noted that according to figure 5, the vacuum pressure of −0.1 bar is the threshold for complete detachment of physical loads below 1.4 N. Therefore, we have kept the sawtooth signal's minimum value above −0.1 bar to enable running repeated experiments consistently. (*b*) The respective sensor signals; note that the added physical load to the bottom of the anchoring module produces a torque about the point of contact during the detachment, and hence a change in the sensing signal (see the inset in figure 5*a* for the setup used for adding physical load to the module). (*c*) The anchor lengths at different loading conditions during detachment. (*d*) Correspondence to the key sequences of detachment, 1 to 4, of the sensory–physical anchoring module with a physical load of 1.09 N. (*e*) Sequence 5 shows the configuration of the anchoring module at the moment of detachment (when the minimum amount of vacuum pressure was reduced to 0). (Online version in colour.)

about the anchor point increases the distance between the optical fibre tip and the contact surface, and hence reduces the sensor signal).

The repeatability of the sensing values is defined as [41]

$$\text{Repeatability} = \left(100 - \frac{\text{standard deviation in repeated measurements}}{\text{sensing range}}\right)\%, \tag{3.1}$$

and is calculated for the anchor length (across five actuation cycles under reverse sawtooth signal) as 93.7%. The standard deviation is computed in Matlab as 0.56 mm and the tactile sensing range is set to 9 mm.

Experimental results shown in figure 6 indicate that the larger loads on the sucker require higher levels of applied vacuum pressure to maintain a stable attachment; this can be seen in that having known values of the sensing signal and the input vacuum signal, the anchoring module is able to discriminate between different values of physical load. However, a blind octopus is not able to distinguish between two objects that are only different in weight using suckers [46]; the weight discrimination ability of the anchoring module can be regarded as an example where bioinspired robotic systems outperform their biological counterparts [47,48].

4. Conclusion

We present a sensory–physical anchoring module with the following mechatronic and material configurations: (1) a stiffness-gradient design in the mechanical structure of artificial infundibulum and acetabulum portions to exploit the softness for conformation to contact surfaces while preserving the viability and mechanical strength of the module and (2) a single sensory unit based on fibre optics integrated into the mechanical structure and calibrated for seamless sensing of the proximity and tactile interactions of the anchoring module with the surrounding environment. While the tactile information can enable assessing the firmness of the anchor(s) to the objects, the proximity information is used to anticipate the approaching objects for robot motion planning prior to the touching event. In order to verify the effectiveness of the proposed anchoring system, a variable set of weights, representing a potential robot body, were attached to the anchoring module and its ability to maintain the anchor was evaluated using the onboard sensing system, under constant and variable vacuum pressure signals. It is shown that the sensory–physical anchoring module is able to quantify the state of firmness of the anchor and discriminate between different amounts of physical load attached to it.

The composition from soft materials is a prominent feature of this anchoring module, unlike more conventional anchoring mechanisms using magnets or pins [49]. The proposed module is highly conformable to surfaces onto which it is attaching itself and can collapse naturally upon collision to avoid any damage to vulnerable substrates. This conformability and softness make it suitable for use as a soft sensory–physical grasper in robotic pick and place applications, especially in food and medicine packaging systems where the hard contact of traditional end-effectors with the delivered substrate is often undesirable. Moreover, the module can assist in many industrial, medical and human participatory applications, e.g. a surgical procedure, where the anchoring device should be capable of performing a gradual attachment/detachment

with characteristics that can warn the operator, e.g. a surgeon, and give them time to react.

Having known values for the physical load, vacuum pressure and number of anchoring modules in a robotic system, future works will consider further development of this concept to create computational models and prototypes of the proposed anchoring concept for locomotion or manipulation in multi-anchor robotic systems applicable to a wide range of medical and industrial applications.

Data accessibility. This article has no additional data.

Authors' contributions. S.S. and M.L. conceived the study. P.S., Y.N. and F.T. contributed to the mechanical, electronics and bioinspired design of the anchoring system. M.L. contributed to the respective simulations. S.S. and M.L. developed the prototype of the anchoring system and performed the experiments. K.A., B.M., and M.K. advised the work, and S.S. wrote the paper.

Competing interests. The authors declare that there is no conflict of interest.

Funding. This work was partly supported by the Seventh Framework Programme of the European Commission under grant agreement 287728 in the framework of EU project STIFF-FLOP.

Endnotes

[1]Merkel cells are oval-shaped mechanoreceptors found in the skin of vertebrates and are essential for fine touch sensing.
[2]The concept of stiffness gradient originates from natural organisms whose body stiffness changes from rigid to soft towards the outer body, such as the structure of bones, muscles and skin in human body.
[3]QTC pills, the most commonly used type of QTC, are pressure sensitive variable resistors that can be used in force/tactile sensing applications.
[4]The moulds were designed in SolidWorks 3D CAD software (SolidWorks Corp.) and 3D printed using a Project HD 3000 3D production system.
[5]Smooth-On Inc., USA.
[6]$\bar{I}_1 = \bar{\lambda}_1^2 + \bar{\lambda}_2^2 + \bar{\lambda}_3^2$ where $\bar{\lambda}_i = J^{-1/3}\lambda_i$ is the deviatoric stretch, λ_i is the principal stretch and J is the total volume ratio [32].
[7]Dassault Systèmes, France.
[8]A custom C# code was developed to synchronously acquire the motor position and values of the sensing signal from the FS-N11MN fibre optic sensor via a NI-USB 6211 DAQ.
[9]A four-core optical fiber bundle produced by Keyence™, USA.
[10]National Instruments™, USA.
[11]MathWorks, Inc., USA.

References

1. Maie T, Schoenfuss HL, Blob RW. 2012 Performance and scaling of a novel locomotor structure: adhesive capacity of climbing gobiid fishes. *J. Exp. Biol.* **215**, 3925–3936. (doi:10.1242/jeb.072967)
2. Wainwright DK, Kleinteich T, Kleinteich A, Gorb SN, Summers AP. 2013 Stick tight: suction adhesion on irregular surfaces in the northern clingfish. *Biol. Lett.* **9**, 20130234. (doi:10.1098/rsbl.2013.0234)
3. Farnesi RM, Marinelli M, Tei S, Vagnetti D. 1981 Morphological and ultrastructural aspects of *Branchiobdella pentodonta* Whit. (Annelida, Oligochaeta) suckers. *J. Morphol.* **170**, 195–205. (doi:10.1002/jmor.1051700206)
4. Stern-Tomlinson W, Nusbaum MP, Perez LE, Kristan WB. 1986 A kinematic study of crawling behavior in the leech, *Hirudo medicinalis*. *J. Comp. Physiol. A* **158**, 593–603. (doi:10.1007/bf00603803)
5. Feng H, Ningli C, Wenhao D. 2015 Experimental investigation on the morphology and adhesion mechanism of leech posterior suckers. *PLoS ONE* **10**, e0140776. (doi:10.1371/journal.pone.0140776)
6. Kampowski T, Eberhard L, Gallenmüller F, Speck T, Poppinga S. 2016 Functional morphology of suction discs and attachment performance of the Mediterranean medicinal leech (*Hirudo verbana* Carena). *J. R. Soc. Interface* **13**, 20160096. (doi:10.1098/rsif.2016.0096)
7. Tessler M, Barrio A, Borda E, Rood-Goldman R, Hill M, Siddall ME. 2016 Description of a soft-bodied invertebrate with microcomputed tomography and revision of the genus *Chtonobdella* (Hirudinea: Haemadipsidae). *Zool. Scr.* **45**, 552–565. (doi:10.1111/zsc.12165)
8. Baader AP. 1997 Interneuronal and motor patterns during crawling behaviour of semi-intact leeches. *J. Exp. Biol.* **200**, 1369–1381.
9. Willms K. 2008 Morphology and biochemistry of the pork tapeworm, *Taenia solium*. *Curr. Top. Med. Chem.* **8**, 375–382. (doi:10.2174/15680260 8783790875)
10. Hochberg FG, Nixon M, Toll RB. 1992 Order OCTOPODA leach, 1818. In *Larval and juvenile cephalopods: a manual for their identification* (eds MJ Sweeney, CFE Roper, KM Mangold, MR Clarke, SV Boletzky), p. 213. Washington, DC: Smithsonian Institution Press.
11. Grasso FW. 2008 Octopus sucker-arm coordination in grasping and manipulation. *Am. Malacol. Bull.* **24**, 13–23. (doi:10.4003/0740-2783-24.1.13)
12. Kier WM, Smith AM. 2002 The structure and adhesive mechanism of octopus suckers. *Integr. Comp. Biol.* **42**, 1146–1153. (doi:10.1093/icb/42.6.1146)
13. Huffard CL. 2006 Locomotion by *Abdopus aculeatus* (Cephalopoda: Octopodidae): walking the line between primary and secondary defenses. *J. Exp. Biol.* **209**, 3697–3707. (doi:10.1242/jeb.02435)
14. Wells MJ. 1978 *Octopus: physiology and behaviour of an advanced invertebrate*, p. 417. London, UK: Chapman & Hall.
15. Grasso FW, Setlur P. 2007 Inspiration, simulation and design for smart robot manipulators from the sucker actuation mechanism of cephalopods. *Bioinspir. Biomim.* **2**, S170–S181. (doi:10.1088/1748-3182/2/4/S06)
16. Robison B, Seibel B, Drazen J. 2014 Deep-sea octopus (*Graneledone boreopacifica*) conducts the longest-known egg-brooding period of any animal. *PLoS ONE* **9**, e103437. (doi:10.1371/journal.pone.0103437)
17. Packard A. 1988 The skin of cephalopods (coleoids): general and special adaptations. In *The mollusca: form and function* (eds ER Trueman, MR Clarke), pp. 37–67. San Diego, CA: Academic Press.
18. Lumelsky VJ. 2005 *Sensing, intelligence, motion: how robots and humans move in an unstructured world*, pp. 399–401. Hoboken, NJ: John Wiley.
19. Marshall KL, Chadha M, deSouza LA, Sterbing-D'Angelo SJ, Moss CF, Lumpkin EA. 2015 Somatosensory substrates of flight control in bats. *Cell Rep.* **11**, 851–858. (doi:10.1016/j.celrep.2015.04.001)
20. Verl A, Alin Albu-Schäffer A, Brock O, Raatz A. 2015 *Soft robotics: transferring theory to application*, pp. 62–63. Berlin, Germany: Springer.
21. Tramacere F, Pugno NM, Kuba MJ, Mazzolai B. 2015 Unveiling the morphology of the acetabulum in octopus suckers and its role in attachment. *Interface Focus* **5**, 20140050. (doi:10.1098/rsfs.2014.0050)
22. Tramacere F, Appel E, Mazzolai B, Gorb SN. 2014 Hairy suckers: the surface microstructure and its possible functional significance in the *Octopus vulgaris* sucker. *Beilstein J. Nanotechnol.* **5**, 561–565. (doi:10.3762/bjnano.5.66)
23. Tramacere F, Beccai L, Kuba M, Gozzi A, Bifone A, Mazzolai B. 2013 The morphology and adhesion mechanism of *Octopus vulgaris* suckers. *PLoS ONE* **8**, e65074. (doi:10.1371/journal.pone.0065074)
24. Tramacere F, Kovalev A, Kleinteich T, Gorb SN, Mazzolai B. 2014 Structure and mechanical properties of *Octopus vulgaris* suckers. *J. R. Soc. Interface* **11**, 20130816. (doi:10.1098/rsif.2013.0816)
25. Tramacere F, Follador M, Pugno NM, Mazzolai B. 2015 Octopus-like suction cups: from natural to artificial solutions. *Bioinspir. Biomim.* **10**, 035004. (doi:10.1088/1748-3190/10/3/035004)
26. Bartlett NW, Tolley MT, Overvelde JTB, Weaver JC, Mosadegh B, Bertoldi K, Whitesides GM, Wood RJ. 2015 A 3D-printed, functionally graded soft robot powered by combustion. *Science* **349**, 161–165. (doi:10.1126/science.aab0129)
27. Sareh S, Jiang A, Faragasso A, Noh Y, Nanayakkara T, Dasgupta P, Seneviratne L, Würdemann H, Althoefer K. 2014 Bio-inspired tactile sensor sleeve for surgical soft manipulators. In *Proc. IEEE Int. Conf.*

on Robotics and Automation, Hong Kong, China, 31 May–7 June 2014, pp. 1454–1459. (doi:10.1109/ICRA.2014.6907043)

28. Hu B, Wang L, Fu Z, Zhao Y. 2009 Bioinspired miniature suction cups actuated by shape memory alloy. *Int. J. Adv. Rob. Syst.* **6**, 151–160. (doi:10.5772/7228)
29. Follador M, Tramacere F, Mazzolai B. 2014 Dielectric elastomer actuators for octopus inspired suction cups. *Bioinspir. Biomim.* **9**, 046002. (doi:10.1088/1748-3182/9/4/046002)
30. Hou J, Bonser R, Jeronimidis G. 2012 Developing sensorized arm skin for an octopus inspired robot. In *2012 IEEE Int. Conf. on Robotics and Automation*, *St Paul, MN, USA, 14–18 May 2012*, pp. 3840–3845. (doi:10.1109/ICRA.2012.6224715).
31. Hou J, Wright E, Bonser RHC, Jeronimidis G. 2012 Development of biomimetic squid-inspired suckers. *J. Bionic Eng.* **9**, 484–493. (doi:10.1016/S1672-6529(11)60144-3)
32. Yeoh OH. 1993 Some forms of the strain energy function for rubber. *Rubber Chem. Technol.* **66**, 754–771. (doi:10.5254/1.3538343)
33. ABAQUS Inc. 2012 Hyperelastic behaviour of rubberlike materials, ABAQUS Analysis User's Manual. Section 22.5.1. See http://abaqus.software.polimi.it/v6.12/pdf_books/ANALYSIS_3.pdf.
34. Huat LG. 2015 Customisable soft pneumatic gripper devices. MSc thesis, National University of Singapore. (http://scholarbank.nus.edu.sg/handle/10635/120577)
35. Zhang B *et al.* 2014 Dual functional transparent film for proximity and pressure sensing. *Nano Res.* **7**, 1488–1496. (doi:10.1007/s12274-014-0510-3)
36. Chen X, Yang S, Sawada N, Motojima S. 2008 The design and performance of tactile/proximity sensors made of carbon microcoils. In *Smart sensors and sensing technology* (eds SC Mukhopadhyay, GS Gupta). Lecture Notes in Electrical Engineering, vol. 20, pp. 251–261. Berlin, Germany: Springer. (doi:10.1007/978-3-540-79590-2_17)
37. Berkovic G, Shafir E. 2012 Optical methods for distance and displacement measurements. *Adv. Optic. Photonic.* **4**, 441–471. (doi:10.1364/AOP.4.000441)
38. Noh Y, Sareh S, Würdemann H, Liu H, Housden J, Rhode K, Althoefer K. 2015 A three-axial fiber-optic body force sensor for flexible manipulators. *IEEE Sens. J.* **99**, 1641–1651. (doi:10.1109/ICRA.2014.6907802)
39. Sareh S, Noh Y, Ranzani T, Liu H, Althoefer K. 2015 A 7.5 mm Steiner chain fiber-optic system for multi-segment flex sensing. In *IEEE/RSJ Int. Conf. on Intelligent Robots and Systems* (*IROS*), *Hamburg, Germany, 28 September–2 October 2015*. (doi:10.1109/IROS.2015.7353692)
40. Konstantinova J, Stilli A, Faragasso A, Althoefer K. 2016 Fingertip proximity sensor with realtime visual-based calibration. In *IEEE/RSJ Int. Conf. on Intelligent Robots and Systems* (*IROS*), *Daejeon, South Korea*, *9–14 October 2016*, pp. 170–175. (doi:10.1109/IROS.2016.7759051)
41. Sareh S, Noh Y, Li M, Ranzani T, Liu H, Althoefer K. 2015 Macrobend optical sensing for pose measurement in soft robot arms. *Smart Mater. Struct.* **24**, 125024. (doi:10.1088/0964-1726/24/12/125024)
42. Wang WC, Ledoux WR, Huang CY, Huang CS, Klute GK, Reinhall PG. 2008 Developments of a microfabricated optical bend loss sensor for distributive pressure measurement. *IEEE Trans. Biomed. Eng.* **55**, 614–625. (doi:10.1109/TBME.2007.912627)
43. Puangmali P, Althoefer K, Seneviratne LD, Murphy D, Dasgupta P. 2008 State-of-the-art in force and tactile sensing for minimally invasive surgery. *IEEE Sens. J.* **8**, 371–381. (doi:10.1109/JSEN.2008.917481)
44. Keyence™. 2017 FS-N Series Digital Fiber Optic Sensors Catalogue. See http://www.keyence.co.uk/products/sensor/fiber-optic/fs-n/features/index.jsp.
45. Gordon RP. 1986 Apparatus for demonstration of negative absolute pressure and ordinary vapour pressures. *J. Chem. Educ.* **63**, 543–544. (doi:10.1021/ed063p543)
46. Wells MJ. 1961 Weight discrimination by octopus. *J. Exp. Biol.* **38**, 127–133.
47. Winter AGV, Hosoi AE. 2011 Identification and evaluation of the Atlantic razor clam (*Ensis directus*) for biologically inspired subsea burrowing systems. *Integr. Comp. Biol.* **51**, 151–157. (doi:10.1093/icb/icr038)
48. Sareh P, Kovac M. 2017 Mechanized creatures. *Science* **355**, 1379. (doi:10.1126/science.aam9075)
49. Kovac M. 2016 Learning from nature how to land aerial robots. *Science* **352**, 895–896. (doi:10.1126/science.aaf6605)